Physics of Fluids

Tuning capillary flow in porous media with hierarchical structures

Cite as: Phys. Fluids **33**, 034107 (2021); https://doi.org/10.1063/5.0038634
Submitted: 26 November 2020 . Accepted: 28 January 2021 . Published Online: 05 March 2021

Si Suo (索思), and Yixiang Gan (甘益翔)

Physics of Fluids ARTICLE scitation.org/journal/phf

Tuning capillary flow in porous media with hierarchical structures

Cite as: Phys. Fluids 33, 034107 (2021); doi: 10.1063/5.0038634
Submitted: 26 November 2020 · Accepted: 28 January 2021 ·
Published Online: 5 March 2021

View Online Export Citation CrossMark

Si Suo (索思),[1] and Yixiang Gan (甘益翔)[1,2,a)]

AFFILIATIONS

[1]School of Civil Engineering, The University of Sydney, Sydney, NSW 2006, Australia
[2]Sydney Nano, The University of Sydney, Sydney, NSW 2006, Australia

[a)]Author to whom correspondence should be addressed: yixiang.gan@sydney.edu.au

ABSTRACT

Immiscible fluid–fluid displacement in porous media is of great importance in many engineering applications, such as enhanced oil recovery, agricultural irrigation, and geologic CO_2 storage. Fingering phenomena, induced by the interface instability, are commonly encountered during displacement processes and somehow detrimental since such hydrodynamic instabilities can significantly reduce displacement efficiency. In this study, we report a possible adjustment in pore geometry, which aims to suppress the capillary fingering in porous media with hierarchical structures. Through pore-scale simulations and theoretical analysis, we demonstrate and quantify the combined effects of wettability and hierarchical geometry on displacement patterns, showing a transition from fingering to compact mode. Our results suggest that with a higher porosity of the second-order porous structure, the displacement can stay compact across a wider range of wettability conditions. Combined with our previous work on viscous fingering in such media, we can provide a complete insight into the fluid-fluid displacement control in hierarchical porous media, across a wide range of flow conditions from capillary- to viscous-dominated modes. The conclusions of this work can benefit the design of microfluidic devices and tailoring porous media for better fluid displacement efficiency at the field scale.

I. INTRODUCTION

Immiscible fluid–fluid displacement in porous media has been widely observed in various scenarios, such as CO_2 sequestration,[1–3] liquid drainage in polymer-based fuel cells,[4] and enhanced oil/gas recovery.[5–7] With the displacement proceeding, fingering phenomena induced by the interface instability may occur, leading to a significant reduction of displacement efficiency and a ramified fluid morphology compared with a compact displacement. Understanding what controls the displacement pattern and furthermore to what extent the fingering can be suppressed is beneficial to all these applications and also essential for estimating the post-displacement status. For instance, the production of oil is directly related to the displacement efficiency and the relative permeability of the residual oil impacts the secondary recovery strategy.[8,9]

The interface instability is a result of combined effects of viscosity and capillarity, which is suggested to be quantified using the capillary number, *Ca*, and viscosity ratio, *M*. Various combinations lead to the displacement pattern transition among viscous fingering, capillary fingering, and compact displacement, as depicted in many phase diagrams.[10–14] Some studies also indicate that altering wettability shows certain potential to suppress fingering phenomena since the capillary effect is directly related to the contact angle,[15] and specifically, the compact mode covers a wider range of regimes when the solid surface is more hydrophilic to the invading fluid.[16–19] However, a recent study by Zhao *et al.*[20] pointed out that for the strong imbibition case, i.e., the surface is of extreme affinity to the invading fluid, displacement instability may be triggered due to the corner flows. Other possible ways, including using non-Newtonian fluids[21,22] or additional electrical fields,[23] can weaken the interface instability for some specific situations.

The geometry of the porous matrix also plays a significant role in the multiphase flow, especially on the pressure distribution and capillary effects.[24–27] For an ordered porous medium, the pore size gradient along the flow direction has been proven an effective approach of suppressing viscous fingering[28] and capillary fingering.[29] For a disordered porous medium, recent studies[30,31] suggested that the displacement tends to be compact with reducing disorder. However, it is still unclear for a given porous media with highly disordered topology that how the displacement pattern is controlled by geometry and to what extent the instability can be mitigated.

Capillary fingering naturally occurs during a capillary force dominated flow characterized typically by $Ca \ll 1$. Different from viscous fingering, the invading morphology of capillary fingering highly depends on the pore geometry[32] especially for the imbibition situation (i.e., the wetting phase invading the nonwetting one) since the interface advances spontaneously along solid surfaces.[33] In addition to different dominating mechanisms in resulting flow patterns in both viscous and capillary regimes, modeling capillary fingering may require much more computational resources due to the significantly slower flow conditions ($Ca \ll 1$). In our recent work,[34] we have demonstrated that the viscous fingering can be suppressed in a homogeneous porous medium by adopting the hierarchical porous structure. Hence, in this work, we investigate the displacement patterns through pore-scale simulations in a capillary-dominated situation, as the complementary piece in understanding the complete flow behavior, with a special focus on adjusting the hierarchical geometry as a possible way to control capillary flows in disordered porous media. The transition from fingering mode to compact mode is demonstrated as in a phase diagram showing the combination of wettability and hierarchical geometry. By analyzing the evolution of related indices during the displacement, we discover the mechanism dominating the fingering suppression and further quantitatively characterize it using a dimensionless number, which incorporates the capillary suction as a driving force instead of the external pressure in a viscous-dominated situation. The current work provides a complete picture on tuning the fluid displacement mode in hierarchical porous media, by drastically extending the capillary number regime by several orders of magnitudes.

II. NUMERICAL METHOD

As proved by many studies,[35,36] the volume of fluid (VOF) method is a well-developed and practical numerical solution for multiphase flow problems at the pore scale. Here, we briefly introduce the governing equations for impressible two-phase flows, i.e., the continuity equation (1), the phase fraction equation (2), and the momentum equation (3) as

$$\nabla \cdot \boldsymbol{u} = 0, \tag{1}$$

$$\frac{\partial \vartheta}{\partial t} + \nabla \cdot (\boldsymbol{u} \cdot \vartheta) + \nabla \cdot \left[\boldsymbol{u}_r \cdot \vartheta \cdot (1-\vartheta)\right] = 0, \tag{2}$$

$$\frac{\partial (\rho \cdot \boldsymbol{u})}{\partial t} + \nabla \cdot (\rho \cdot \boldsymbol{u} \cdot \boldsymbol{u}) - \nabla \cdot (\mu \cdot \nabla \boldsymbol{u}) - (\nabla \boldsymbol{u}) \cdot \nabla \mu = -\nabla p + \gamma \cdot \kappa \cdot \nabla \vartheta, \tag{3}$$

where ϑ is the phase fraction of two fluids, $\boldsymbol{u}$ is the weighted average of the velocity field shared by two fluids, i.e., $\boldsymbol{u} = \vartheta \cdot \boldsymbol{u}_{f1} + (1-\vartheta) \cdot \boldsymbol{u}_{f2}$, and $\boldsymbol{u}_r$ is the relative velocity, i.e., $\boldsymbol{u}_r = \boldsymbol{u}_{f1} - \boldsymbol{u}_{f2}$, ρ and μ represent the weighted average of density and viscosity, respectively, i.e., $\rho = \vartheta \cdot \rho_{f1} + (1-\vartheta) \cdot \rho_{f2}$ and $\mu = \vartheta \cdot \mu_{f1} + (1-\vartheta) \cdot \mu_{f2}$, p is the pressure, γ is the surface tension, and κ is the mean curvature of the interface between two fluids. Equations (1)–(3) are solved using OpenFoam, an open source CFD toolbox, and for more details regarding the treatment of inlet-outlet boundaries and wetting conditions of solid surfaces, one can refer to Refs. 37 and 38.

Our study is on a 2D domain initially saturated with the defending phase and then displaced from the left (see Fig. 1). The left side is a uniformly inlet boundary with a fixed flow rate, while the outlet boundary on the right side is set with a total pressure value $p_{\text{out}} = 0$ Pa; the top and bottom sides are no-slip walls with a contact angle of 90°.

In this study, we focus on the capillary-dominated displacement processes. The invading and defending fluids have the same viscosity $\eta = 1$ mPa·s, density $\rho = 1 \times 10^3$ kg/m^3, and surface tension between two fluids, $\gamma = 28.2$ mN/m; meanwhile, the inlet flow rate is limited as a very small value, i.e., $v_{in} = 1 \times 10^{-3}$ mm/s, so that the viscosity ratio $M = 1$ and capillary number $Ca = 3.55 \times 10^{-8}$. Note that modeling the capillary-dominate regime is quite computationally intensive due

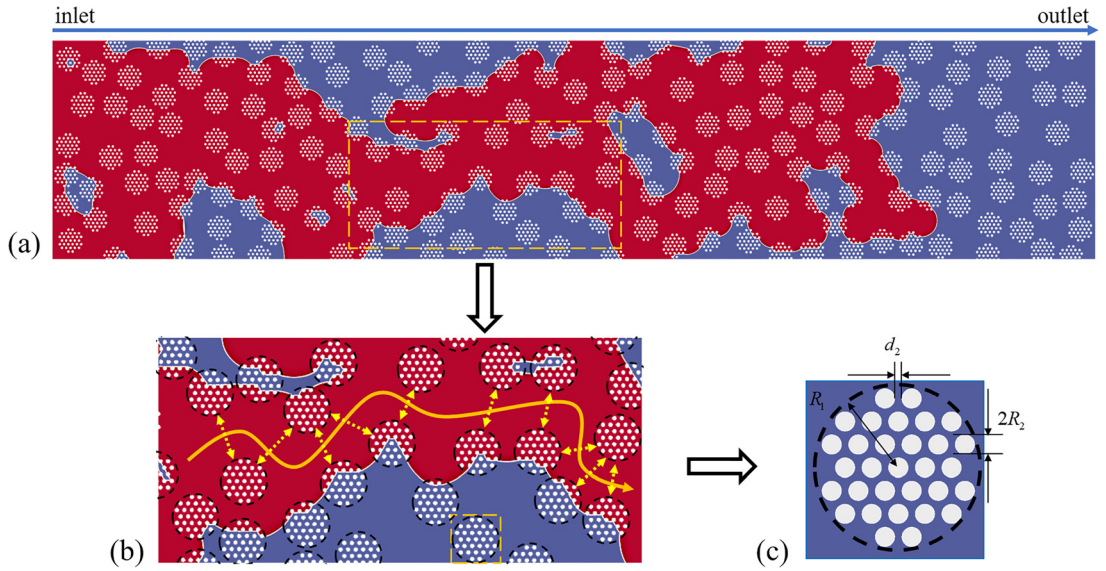

FIG. 1. (a) The numerical model with two-level hierarchical porous media, i.e., (b) first-order disordered and (c) second-order homogeneous porous structures.

to the extreme slow flow rate and extensive simulation time. According to the phase diagram of fluid–fluid displacement patterns,[14] such a combination of M and Ca lies within the capillary fingering regime. The stability of a fluid-fluid displacement also depends on the topology of solid obstacles as suggested in Ref. 30, and specifically, the displacement process tends to be instable with a larger disorder index I_v. Thus, through the Mont Carlo iteration, we here generate a 2D domain without out-of-plane flow or gradients, containing randomly distributed round obstacles with radius $R_1 = 0.8$ mm with $I_v = 0.052$, as shown in Fig. 1, which can guarantee the capillary fingering to occur during the weak imbibition (contact angle $\theta > 30°$). To shed light on the effect of hierarchical structures on displacement patterns, each obstacle has an identical homogeneous porous structure with the second-order throat size (d_2) equaling 0.06, 0.112, 0.144, and 0.160 mm, and the corresponding geometry parameters, including the particle radius (R_2), porosity (ϕ_2), and permeability (k_2), are listed in Table I. Moreover, the simulations are performed with a group of contact angles θ measured within the invading phase, i.e., ranging from 30° to 90° to cover a wide range of wettability conditions. The interval of contact angle is later refined in specific regions to illustrate the transition of displacement modes in Sec. III.

III. RESULTS AND DISCUSSION

Generally, a fluid–fluid displacement process can be divided into pre- and post-breakthrough stages, i.e., split by the moment when the invading front reaches the outlet. The global channels for the invading phase are built at the pre-breakthrough stage and remain mostly at the post-breakthrough stage; only the local fluid distribution may be rearranged due to the unbalance of capillary pressures, and such capillary rearrangement can last for a relatively long time during the post-breakthrough stage.[39] The contrast between the durations of these two time periods in viscous fingering can be notable, while in capillary fingering, the global and local balance can be acquired in similar time scales. Furthermore, considering that the major flow patterns can be characterized at the early evolution, we only investigate the displacement processes before the breakthrough in this study.

A. Phase diagram

Capillary-dominated displacement is generally regarded as a percolation-like process,[33] i.e., the slow invasion advances pore by pore and prefers the pathway with the lowest entry capillary pressure. The geometric disorder leads to nonuniformly distributed capillary pressure and finally causes phase trapping and fingering. However, in hierarchical porous media, such a macroscopic pathway-bias may be balanced due to second-order porous structures. Specifically, under the same flow condition, the displacement pattern may transit from the fingering to compact mode by adjusting the second-order geometry. The effects of hierarchical geometry on a capillary-dominated displacement under various wetting conditions from strong to neutral imbibition are summarized as a phase diagram in Fig. 2. The displacement pattern can transit from the compact to fingering mode with increasing contact angle θ,[16] which agrees with the observation for each geometry as shown in Fig. 2. However, with fixed wetting conditions, cases with different second-order porous structures may present evidently distinct displacement processes, especially within the regime of weak and neutral imbibition ($\theta = 60° - 90°$). In another word, the mode transition for each geometry shows different sensitivities to the wetting conditions though the crossover boundary mostly lies within the weak imbibition regime ($45° < \theta < 90°$), and specifically, for dense packing cases ($\phi_2 < 0.8$) at the second-order porous structure, the crossover boundary is at around $\theta \approx 53°$, while for loose packing cases ($\phi_2 > 0.8$), the critical contact angle θ is $> 60°$, i.e., the fingering mode can be suppressed within a larger range of the weak imbibition regime for the loose packing cases. Correspondingly, even under the same wetting conditions where the fingering mode occurs, the displacement process demonstrates relatively high stability in cases with loosely packed obstacles. Since the capillary number in this simulation is small enough so that the capillary effects govern the whole displacement, the dynamics of the fluid-fluid interface is mostly driven by the capillary pressure, which is determined by the pore geometry and contact angle. Before spontaneously infiltrating the pore space, the external pressure should be larger than the entry capillary pressure at the throat. For loose packing cases, the capillary effect is weaker, i.e., the entry capillary pressure is lower, while the spontaneous driving pressure is also lower than that in dense packing cases under fixed wetting conditions. The competition between the entry capillary resistance and spontaneous infiltrating leads to the transition between the above two displacement modes. Notably, for the strong imbibition regime ($\theta \leq 30°$), although the compact displacement occurs in all cases, there exist certain noticeable differences among them, especially in the case with $\phi_2 = 0.47$ and $\theta = 30°$, as shown in Fig. 2(c), and more defending fluid is trapped within first pore space along the top and bottom walls during the displacement, while almost a perfect compact displacement occurs in other cases under the same wetting conditions. Since the negative capillary pressure is quite larger along the narrow channels in the strong imbibition regime, the interface in the case with $\phi_2 = 0.47$ moves so much faster through the second-order porous structure than along the walls or through the first-order pore space that defending phase is left behind and trapped finally. This phenomenon is similar to the corner flow reported in Refs. 17 and 20, i.e., the invading fluid advances preferentially along narrow corners due to the intensive capillary effects resulting in local instability.

In summary, during a capillary-dominated displacement process, the strong capillary effects may lead to instability, and specifically, the global fingering pattern occurs in the weak and neutral imbibition regime, while the local instability like trapping of the defending phase arises in the strong imbibition regime. In particular, for hierarchical porous media, the transition of displacement modes can be controlled by adjusting the second-order geometry, and the fingering mode can be suppressed within a large range of wetting conditions for cases with loosely packed obstacles.

TABLE I. Geometry parameters for the second-order pore structures, with $\phi_1 = 0.64$ and $R_1 = 0.8$ mm.

d_2 (mm)	R_2 (mm)	ϕ_2	k_2 (mm^2)[a]
0.060	0.105	0.47	2.34×10^{-4}
0.112	0.079	0.70	1.27×10^{-3}
0.144	0.0626	0.81	2.62×10^{-3}
0.160	0.0556	0.85	3.60×10^{-3}

[a]Permeability k_2 is a function of d_2 and ϕ_2, and its calculation can be referred in Ref. 34.

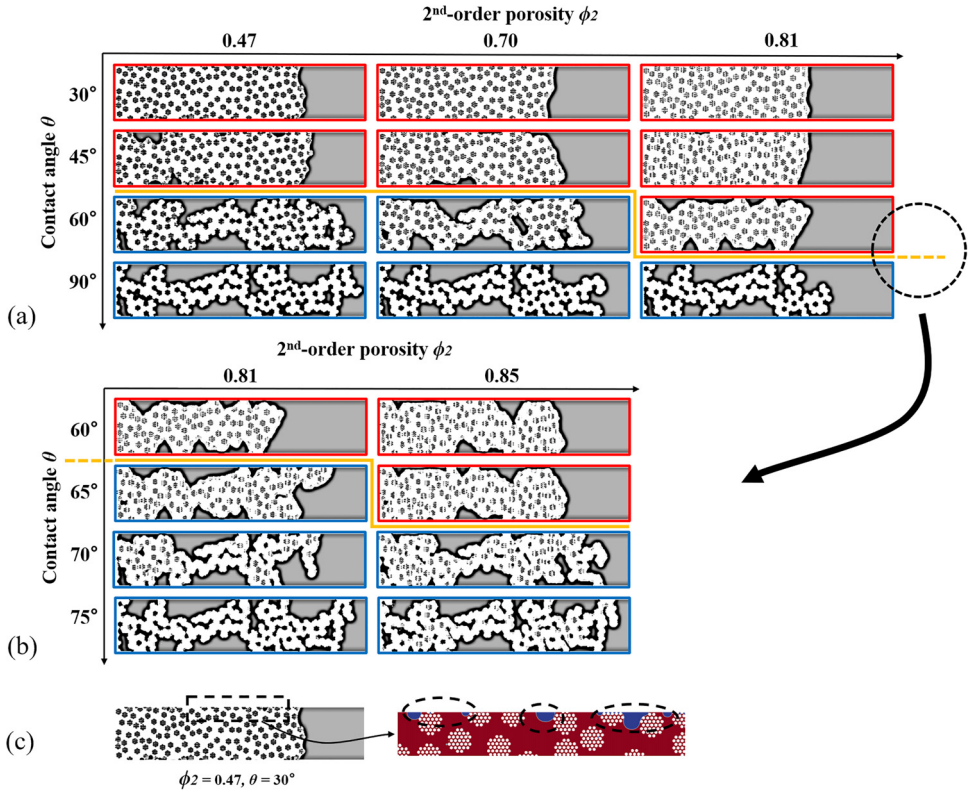

FIG. 2. Phase diagrams (a) and (b) of displacement mode transition between the compact mode (red squares) and the fingering mode (blue squares) in hierarchical porous media with various second-order geometry designs and different wetting conditions, and the yellow line indicates the position of the crossover boundary. (c) A zoom-in view of trapped defending fluid in the case with $\phi_2 = 0.47$ and $\theta = 30^\circ$.

B. Temporal evolutions

To quantitatively characterize the fluid-fluid displacement processes in hierarchical porous media and demonstrate the different displacement modes, a set of indexes are extracted from each time frame and demonstrated in Fig. 3.

(I) The relative fluid–fluid interface length (L_i), i.e., the total interface length normalized by the domain width, is a good indicator to distinguish two displacement modes. Specifically, L_i should be around unity for compact displacement since the invading front is almost parallel to the short side of the domain, while it becomes much larger once dendrites are formed and grow. On the other hand, L_i can also reflect the local instability since it is much sensitive to the fluid trapping, e.g., as shown in Fig. 3(a), for the compact displacement, L_i in the case with $\phi_2 = 0.47$ increases faster with respect to the injecting time than that in other cases because of the trapped defending ganglia marked in Fig. 2(c). Considering that L_i presents a linear relationship with the injecting time for each case, the growth rate $k_{int} = \mathrm{d}L_i/\mathrm{d}t$ is extracted here to characterize the process.

(II) Fractal dimension D_f, measured using the box counting algorithm,[40] can estimate the overall compactness of invading fluid distribution, i.e., that D_f is close to 2 suggests that the domain is being filled with the invading phase uniformly; on the contrary, the fluid trapping or dendrite growth may occur with D_f of smaller values. For each case with the displacement evolving, D_f tends to reach a constant level $\tilde{D}_f$ after 10 000 s, as shown in Fig. 3(b). The crossover boundary marked in Figs. 2(a) and 2(b) corresponds to a stable level of $\tilde{D}_f \approx 1.95$.

(III) Evolution of degrees of saturation for the invading fluid in the second-order (S_2) and first-order (S_1) pore space describes to what extend the invading fluid infiltrates the second-order pore space when the fluid advances through the main channels in the first-order porous structure. Considering that the secondary channels in the wetted second-order pore space can connect the neighboring main channels in the first-order pore space, the second-order saturation, S_2, in effect contributes to the relative permeability of the invading fluid, and furthermore with higher values of S_2, the disorder-induced nonuniform distribution of capillary pressure can be mitigated and the instability be suppressed as a result. As shown in Fig. 3(c), S_2 is almost linearly proportional to S_1 for each case, and the slope k_{sat} is used here to measure the involvement of second-order porous structures during the displacement process. The simulation results suggest that when k_{sat} is larger than 0.9,

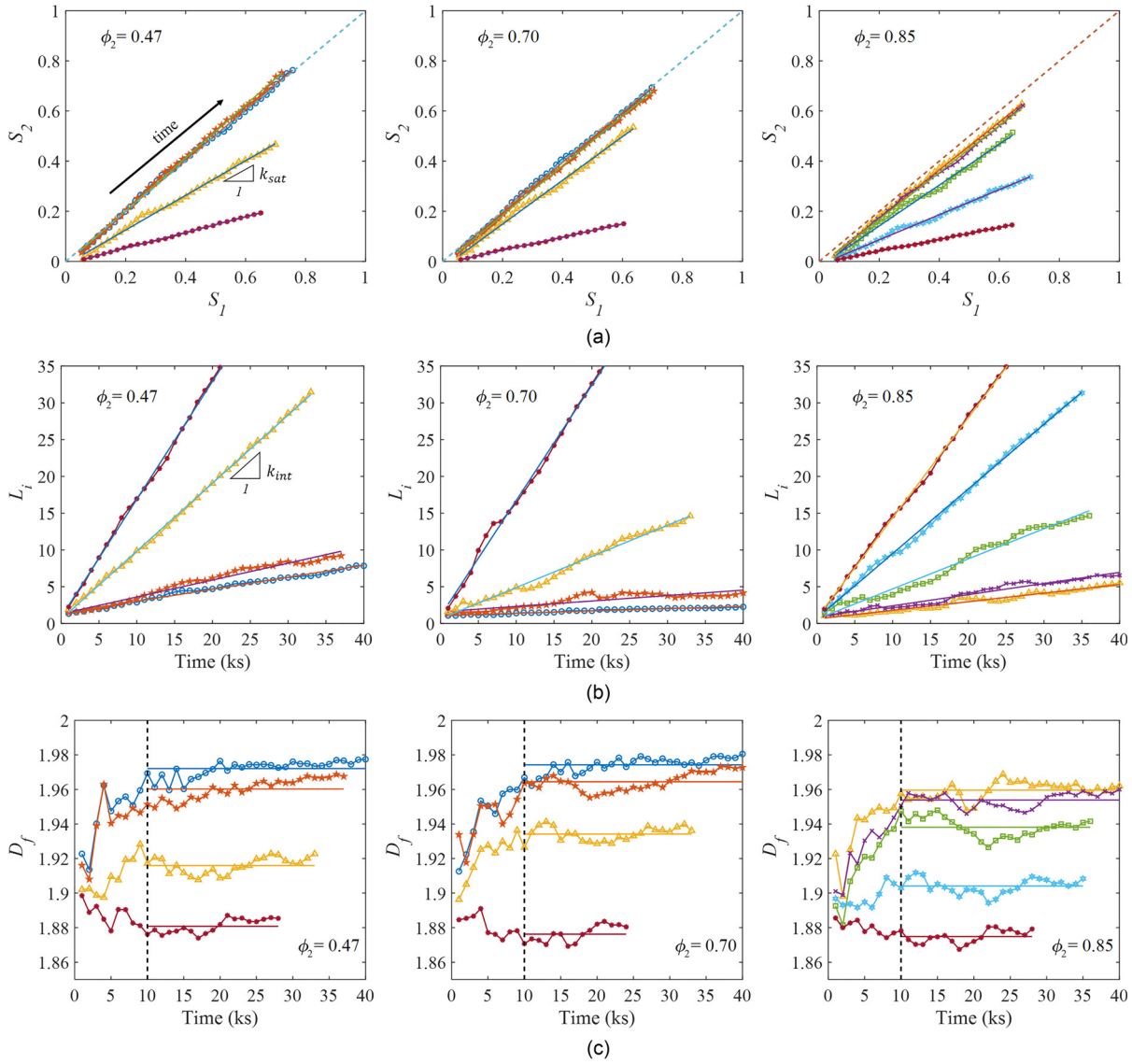

FIG. 3. The evolutions of displacement indexes: (a) the relative fluid–fluid interface length L_i vs injecting time; (b) the fractal dimension D_f vs injecting time, and the dashed line (– – –) indicates that the fractal dimension almost keeps a steady level after the marked moment; and (c) saturation in second-order pore space S_2 vs in 1st-order pore space S_1, and the dashed line (– – –) indicates $S_2 = S_1$. Circle: $\theta = 30°$, five-pointed star: $\theta = 45°$, triangle: $\theta = 60°$, cross: $\theta = 65°$, square: $\theta = 70°$, six-pointed star: $\theta = 75°$, asterisk: $\theta = 90°$, and solid line: fitting line.

the displacement tends to be compact, while the porous obstacle behaves like solid one when k_{sat} is smaller than 0.4 so that the fingering may occur.

C. Dimensionless analysis

Based on the observation of Fig. 2 and analysis on characterization of the displacement patterns, the mode transition is determined by two factors: one is the interaction time, which connects the first-order and second-order flows in hierarchical porous media, and the other is the capillary competition between entry resistance and spontaneous driving force.

1. Interaction time

The mechanism for fingering suppressing is that the infiltrated secondary channels in second-order pore space enhance the global permeability of the invading phase by connecting the main channels in first-order pore space, resulting in the mitigation of distribution nonuniformity of capillary pressure. So, the displacement pattern is controlled by how much invading fluid can infiltrate the second-order pore space when the front advances through the first-order channels. To exactly reflect such effects, we use a characterized timescale ratio R_T of similar expression with our previous work,[34] i.e., the time (T_{1st}) for invading the front advancing a certain characteristic distance

(e.g., R_1) in first-order pore space and that (T_{2nd}) for capillary-driven infiltration in second-order pore space as

$$T_{1st} = \frac{R_1}{v_{in}}, \tag{4}$$

$$T_{2nd} = \frac{\eta \phi_2 R_1}{2 k_2 P_c^*}, \tag{5}$$

where P_c^* is the characteristic capillary pressure estimated by

$$P_c^* = \frac{\int_{-\pi/2}^{\pi/2} P_c(\alpha) d\alpha}{\pi}, \text{and} \tag{6}$$

$$P_c = \frac{\gamma}{d_2} \frac{\cos(\theta - \alpha)}{1 + 2R_2/d_2(1 - \cos(\alpha))}. \tag{7}$$

The calculation model for capillary pressure as a function of filling angle α in Eq. (7) is that the interface advances through two cylinders with radius R_2 and gap distance d_2, and more details can be referred to Ref. 34 Notably, the expression of P_c^* adopted here is different from the one in Ref. 34. The previous expression is more sensitive to the wettability, especially for the case with a smaller second-order porosity when θ is close to 90° because the contribution of negative capillary pressure is truncated by a reduced range of integration. Unlike the previous study in which the capillary effect only dominates the flow in the second-order pore space, in this study, the flow in both the first and second-order pore space is dominated by such effects. Thus, the current expression can provide a more reasonable estimation for the capillary effect. Finally, the time ratio, R_T, can be expressed as

$$R_T = \frac{T_{1st}}{T_{2nd}} = \frac{2 k_2 P_c^*}{\phi_2 v_{in} \eta R_1}. \tag{8}$$

According to Eq. (8), R_T describes the interaction between two characteristic scales by combining the forced flow in the first-order porous structure and spontaneous flow in second-order pore space. With a larger R_T, more secondary channels are expected to be filled with the invading fluid, spontaneously leading to a more compact displacement. However, the capillary effect in Eq. (8) is just roughly estimated. By considering that the entry capillary pressure also controls the spontaneous infiltration of the invading fluid, R_T should be further modified.

2. Capillary competition

When the invading fluid enter a pore body through a narrow throat, the negative capillary pressure acting as a resistance at the entry should be conquered first; when the pressure difference is larger than such threshold capillary pressure, the meniscus moves along the pore throat driven by the capillary pressure, and a possible capillary event, i.e., burst, touch, or overlap, occurs when entering the pore body.[41] Thus, we propose another pressure ratio, R_c, to describe the competition between capillary resistance and spontaneous driving, i.e.,

$$R_c = \frac{P_c^{\max}}{P_c^{\min}}, \tag{9}$$

where $P_c^{\max}$ and $P_c^{\min}$ are the maximum and minimum capillary pressures in Eq. (7), respectively. Combining R_T and R_c, we obtain a complete description of effects on capillary-dominated fluid-fluid displacement in hierarchical porous media, and a so-called "hierarchical number" is expressed as

$$\mathrm{Hi}^c = R_T \cdot R_c. \tag{10}$$

Compared to the hierarchical number proposed in our previous work for viscous fingering,[34] besides some similarities in constructing both hierarchical numbers, Hi^c here shows certain variation on terms. Specifically, the physical meaning of the pressure ratio becomes different. For capillary fingering with a low capillary number, P_c^{min} represents the entry capillary resistance, while P_c^{max} is a characteristic value of capillary-induced driving force, so the ratio R_c describes to what extent the meniscus can move spontaneously, i.e., driven by capillary pressure and specifically, with R_c increasing, the capillary resistance is relatively weak, while the driving effect becomes stronger. However, for viscous fingering with a high capillary number, the flow in the first-order porous structure is mainly forced by the external pressure, while capillary suction is present in the second-order porous structures, so its pressure ratio describes to what extent the barrier pressure can be conquered by the external inject. For both viscous and capillary fingering cases, with a larger hierarchical number, more connections of invading fluid can be established during displacement so that instability induced by the disorder of obstacle arrangement in the capillary-dominated situation, or by viscosity variation in the viscous-dominated situation, can be alleviated.

D. Correlation analysis

To further quantify the relationship between the proposed hierarchical number and displacement patterns, the adopted indexes in Sec. III B as a function of Hi^c are demonstrated in Fig. 4. The crossover boundary shown in Fig. 2 corresponds to $\mathrm{Hi}^c = 6.5 \times 10^8$. Overall, as shown in Fig. 4, all indexes present a monotonous variation with Hi^c. Specifically, the growth rate of the interface length, k_{int}, is inversely proportional to Hi^c; the relationship between Hi^c and stable fractal dimension $\tilde{D}_f$ or the second-order saturation rise rate, k_{sat}, is an S-shaped curve, which marks the upper and lower bounds as two asymptotes corresponding to the extreme values in compact and fingering modes, respectively. Compared to the monotonically decreasing curve of k_{int}, the upper asymptote in S-shape curves suggests that $\tilde{D}_f$ and k_{sat} cannot reflect the slight difference induced by local instability like fluid trapping presented in the strong imbibition regime.

IV. CONCLUSION

This work focuses on the capillary-dominated displacement pattern in hierarchical porous media. Besides the effects of the wettability and geometrical disorder, we mainly investigated the impacts of hierarchical geometry on the transition of displacement modes through a series of pore-scale simulations. Based on the simulation results, the following conclusions can be reached:

(1) The displacement pattern can be classified into the compact mode and fingering mode, and a phase diagram, demonstrating the mode transition under combined conditions of wettability and geometry features, suggests that weakening the capillary effects by increasing the second-order porosity can enhance the displacement stability.

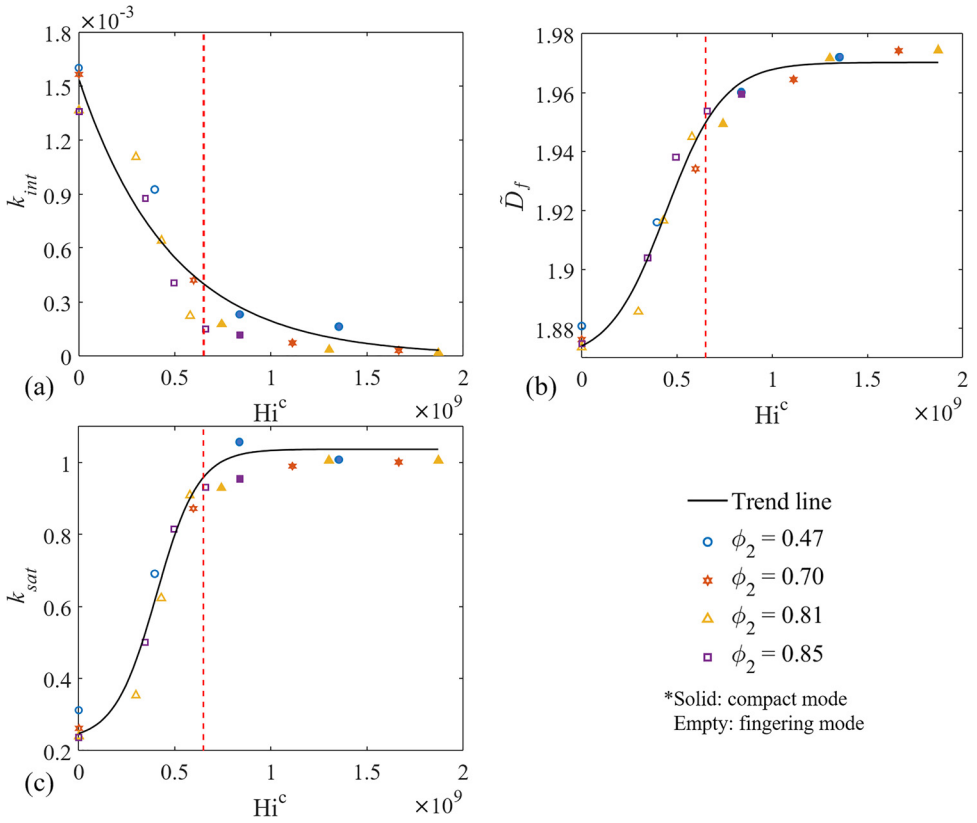

FIG. 4. Flow pattern indexes vs hierarchical number, i.e., (a) growth rate of the interface length, k_{int}; (b) fractal dimension, $\tilde{D}_f$; and (c) rise rate of second-order saturation with 1st-order saturation, k_{sat}. The crossover boundary is marked by the dashed line, as $\mathrm{Hi}^c = 6.5 \times 10^8$.

(2) The mechanism of fingering suppressing is clarified based on the analysis regarding the displacement-related indexes, and specifically, the wetted second-order porous space may bring in extra connections within invading fluid, leading to a more uniform distribution of capillary pressure, so that the interface advances in a stable and compact mode.
(3) Finally, a dimensionless number (Hi^c) is proposed here to quantitatively estimate the involvement of second-order pore space during the displacement by considering capillary-induced resistance and driving force together.

Complimented with the work on viscous fingering, we can provide a complete picture on the fluid–fluid displacement control, and specifically, if fingering is expected to be suppressed in a capillary-dominated situation, the capillary effects should be weakened, e.g., by loosening the packing in second-order space; inversely, if in a viscous-dominated situation, the capillary effects should be enhanced, e.g., densifying the packing in second-order space. Since the hierarchical porous structure is commonly encountered in nature and applications,[42–44] the mechanism of displacement transition may contribute to linking the pore-scale observation with the multiphase flow at the field scale. In addition, this study has also potential to benefit the design of microfluidic devices[45–47] to have tailored flow patterns.

SUPPLEMENTARY MATERIAL

See the supplementary material for the animations for dynamic processes of fluid-fluid displacement.

DATA AVAILABILITY

The data that support the findings of this study are available from the corresponding authors upon reasonable request.

REFERENCES

[1]Z. Zhang, S.-Y. Pan, H. Li, J. Cai, A. G. Olabi, E. J. Anthony, and V. Manovic, "Recent advances in carbon dioxide utilization," Renewable Sustainable Energy Rev. **125**, 109799 (2020).
[2]A. Alhosani, A. Scanziani, Q. Lin, A. Q. Raeini, B. Bijeljic, and M. J. Blunt, "Pore-scale mechanisms of CO_2 storage in oilfields," Sci. Rep. **10**, 8534 (2020).
[3]A. H. Kohanpur, M. Rahromostaqim, A. J. Valocchi, and M. Sahimi, "Two-phase flow of CO2-brine in a heterogeneous sandstone: Characterization of the rock and comparison of the lattice-Boltzmann, pore-network, and direct numerical simulation methods," Adv. Water Resour. **135**, 103469 (2020).
[4]Y. Wang, K. S. Chen, J. Mishler, S. C. Cho, and X. C. Adroher, "A review of polymer electrolyte membrane fuel cells: Technology, applications, and needs on fundamental research," Appl. Energy **88**, 981 (2011).
[5]Q. Gu, L. Zhu, Y. Zhang, and H. Liu, "Pore-scale study of counter-current imbibition in strongly water-wet fractured porous media using lattice Boltzmann method," Phys. Fluids **31**, 086602 (2019).

[6]Y. Liu, J. Cai, M. Sahimi, and C. Qin, "A study of the role of microfractures in counter-current spontaneous imbibition by lattice Boltzmann simulation," Transp. Porous Media **133**, 313 (2020).
[7]M. R. Rokhforouz and H. A. Akhlaghi Amiri, "Phase-field simulation of counter-current spontaneous imbibition in a fractured heterogeneous porous medium," Phys. Fluids **29**, 062104 (2017).
[8]M. Khishvand, A. H. Alizadeh, I. Oraki Kohshour, M. Piri, and R. S. Prasad, "In situ characterization of wettability alteration and displacement mechanisms governing recovery enhancement due to low-salinity waterflooding," Water Resources Res. **53**, 4427 (2017).
[9]R. Aziz, V. Niasar, H. Erfani, and P. J. Martínez-Ferrer, "Impact of pore morphology on two-phase flow dynamics under wettability alteration," Fuel **268**, 117315 (2020).
[10]C. Zhang, M. Oostrom, T. W. Wietsma, J. W. Grate, and M. G. Warner, "Influence of viscous and capillary forces on immiscible fluid displacement: Pore-scale experimental study in a water-wet micromodel demonstrating viscous and capillary fingering," Energy Fuels **25**, 3493 (2011).
[11]U. Bandara, A. M. Tartakovsky, M. Oostrom, B. J. Palmer, J. Grate, and C. Zhang, "Smoothed particle hydrodynamics pore-scale simulations of unstable immiscible flow in porous media," Adv. Water Resour. **62**, 356 (2013).
[12]Y. F. Chen, S. Fang, D. S. Wu, and R. Hu, "Visualizing and quantifying the crossover from capillary fingering to viscous fingering in a rough fracture," Water Resources Res. **53**, 7756 (2017).
[13]M. Ferer, C. Ji, G. S. Bromhal, J. Cook, G. Ahmadi, and D. H. Smith, "Crossover from capillary fingering to viscous fingering for immiscible unstable flow: Experiment and modeling," Phys. Rev. E **70**, 016303 (2004).
[14]Y.-F. Chen, D.-S. Wu, S. Fang, and R. Hu, "Experimental study on two-phase flow in rough fracture: Phase diagram and localized flow channel," Int. J. Heat Mass Transfer **122**, 1298 (2018).
[15]J. Xiao, Y. Luo, M. Niu, Q. Wang, J. Wu, X. Liu, and J. Xu, "Study of imbibition in various geometries using phase field method," Capillarity **2**, 57 (2019).
[16]M. Trojer, M. L. Szulczewski, and R. Juanes, "Stabilizing fluid-fluid displacements in porous media through wettability alteration," Phys. Rev. Appl. **3**, 054008 (2015).
[17]R. Hu, J. Wan, Z. Yang, Y. F. Chen, and T. Tokunaga, "Wettability and flow rate impacts on immiscible displacement: A theoretical model," Geophys. Res. Lett. **45**, 3077, https://doi.org/10.1002/2017GL076600 (2018).
[18]T. Lan, R. Hu, Z. Yang, D.-S. Wu, and Y.-F. Chen, "Transitions of fluid invasion patterns in porous media," Geophys. Res. Lett. **47**, e2020GL089682, https://doi.org/10.1029/2020GL089682 (2020).
[19]F. G. Wolf, D. N. Siebert, and R. Surmas, "Influence of the wettability on the residual fluid saturation for homogeneous and heterogeneous porous systems," Phys. Fluids **32**, 052008 (2020).
[20]B. Zhao, C. W. MacMinn, and R. Juanes, "Wettability control on multiphase flow in patterned microfluidics," Proc. Natl. Acad. Sci. U. S.A. **113**, 10251 (2016).
[21]M. A. Nilsson, R. Kulkarni, L. Gerberich, R. Hammond, R. Singh, E. Baumhoff, and J. P. Rothstein, "Effect of fluid rheology on enhanced oil recovery in a microfluidic sandstone device," J. Non-Newtonian Fluid Mech. **202**, 112 (2013).
[22]C. Xie, W. Lv, and M. Wang, "Shear-thinning or shear-thickening fluid for better EOR?—A direct pore-scale study," J. Pet. Sci. Eng. **161**, 683 (2018).
[23]T. Gao, M. Mirzadeh, P. Bai, K. M. Conforti, and M. Z. Bazant, "Active control of viscous fingering using electric fields," Nat. Commun. **10**, 4002 (2019).
[24]R. T. Armstrong and S. Berg, "Interfacial velocities and capillary pressure gradients during Haines jumps," Phys. Rev. E **88**, 043010 (2013).
[25]A. Ferrari and I. Lunati, "Direct numerical simulations of interface dynamics to link capillary pressure and total surface energy," Adv. Water Resour. **57**, 19 (2013).
[26]H. S. Suh, D. H. Kang, J. Jang, K. Y. Kim, and T. S. Yun, "Capillary pressure at irregularly shaped pore throats: Implications for water retention characteristics," Adv. Water Resour. **110**, 51 (2017).
[27]J. Cai, E. Perfect, C.-L. Cheng, and X. Hu, "Generalized modeling of spontaneous imbibition based on Hagen–Poiseuille flow in tortuous capillaries with variably shaped apertures," Langmuir **30**, 5142 (2014).
[28]H. S. Rabbani, D. Or, Y. Liu, C.-Y. Lai, N. B. Lu, S. S. Datta, H. A. Stone, and N. Shokri, "Suppressing viscous fingering in structured porous media," Proc. Nat. Acad. Sci. U. S. A. **115**, 4833 (2018).
[29]N. B. Lu, C. A. Browne, D. B. Amchin, J. K. Nunes, and S. S. Datta, "Controlling capillary fingering using pore size gradients in disordered media," Phys. Rev. Fluids **4**, 084303 (2019).
[30]Z. Wang, K. Chauhan, J.-M. Pereira, and Y. Gan, "Disorder characterization of porous media and its effect on fluid displacement," Phys. Rev. Fluids **4**, 034305 (2019).
[31]R. Holtzman, "Effects of pore-scale disorder on fluid displacement in partially-wettable porous media," Sci. Rep. **6**, 36221 (2016).
[32]M. Cieplak and M. O. Robbins, "Influence of contact angle on quasistatic fluid invasion of porous media," Phys. Rev. B **41**, 11508 (1990).
[33]M. Alava, M. Dubé, and M. Rost, "Imbibition in disordered media," Adv. Phys. **53**, 83 (2004).
[34]S. Suo, M. Liu, and Y. Gan, "Fingering patterns in hierarchical porous media," Phys. Rev. Fluids **5**, 034301 (2020).
[35]A. Q. Raeini, M. J. Blunt, and B. Bijeljic, "Modelling two-phase flow in porous media at the pore scale using the volume-of-fluid method," J. Comput. Phys. **231**, 5653 (2012).
[36]A. Q. Raeini, B. Bijeljic, and M. J. Blunt, "Numerical modelling of sub-pore scale events in two-phase flow through porous media," Transp. Porous Media **101**, 191 (2014).
[37]C. W. Hirt and B. D. Nichols, "Volume of fluid (VOF) method for the dynamics of free boundaries," J. Comput. Phys. **39**, 201 (1981).
[38]S. W. J. Welch and J. Wilson, "A volume of fluid based method for fluid flows with phase change," J. Comput. Phys. **160**, 662 (2000).
[39]C. Odier, B. Levaché, E. Santanach-Carreras, and D. Bartolo, "Forced imbibition in porous media: A fourfold scenario," Phys. Rev. Lett. **119**, 208005 (2017).
[40]L. S. Liebovitch and T. Toth, "A fast algorithm to determine fractal dimensions by box counting," Phys. Lett. A **141**, 386 (1989).
[41]R. Hu, T. Lan, G.-J. Wei, and Y.-F. Chen, "Phase diagram of quasi-static immiscible displacement in disordered porous media," J. Fluid Mech. **875**, 448 (2019).
[42]J.-Y. Huang, H. Xu, E. Peretz, D.-Y. Wu, C. K. Ober, and T. Hanrath, "Three-dimensional printing of hierarchical porous architectures," Chem. Mater. **31**, 10017 (2019).
[43]L. Alison, S. Menasce, F. Bouville, E. Tervoort, I. Mattich, A. Ofner, and A. R. Studart, "3D printing of sacrificial templates into hierarchical porous materials," Sci. Rep. **9**, 409 (2019).
[44]P. Trogadas, M. M. Nigra, and M.-O. Coppens, "Nature-inspired optimization of hierarchical porous media for catalytic and separation processes," New J. Chem. **40**, 4016 (2016).
[45]X. Chen, T. Li, J. Shen, and Z. Hu, "Fractal design of microfluidics and nanofluidics—A review," Chemom. Intell. Lab. Syst. **155**, 19 (2016).
[46]K. Ren, J. Zhou, and H. Wu, "Materials for microfluidic chip fabrication," Acc. Chem. Res. **46**, 2396 (2013).
[47]E. Y. Kenig, Y. Su, A. Lautenschleger, P. Chasanis, and M. Grünewald, "Microseparation of fluid systems: A state-of-the-art review," Sep. Purif. Technol. **120**, 245 (2013).